



## Anti-diabetic and anti-parasitic properties of a family of luminescent zinc coordination compounds based on the 7-amino-5-methyl-1,2,4-triazolo[1,5-*a*]pyrimidine ligand

Ginés M. Esteban-Parra<sup>a</sup>, Eider San Sebastián<sup>b</sup>, Javier Cepeda<sup>b</sup>, Cristina Sánchez-González<sup>c,\*</sup>, Lorenzo Rivas-García<sup>c</sup>, Juan Llopis<sup>c</sup>, Pilar Aranda<sup>c</sup>, Manuel Sánchez-Moreno<sup>d</sup>, Miguel Quirós<sup>a,\*</sup>, Antonio Rodríguez-Diéguez<sup>a,\*</sup>

<sup>a</sup> Dept. of Inorganic Chemistry, University of Granada, C/Severo Ochoa s/n, 18071 Granada, Spain

<sup>b</sup> Departamento de Química Aplicada, Facultad de Química, University of The Basque Country (UPV/EHU), 20018 San Sebastian, Spain

<sup>c</sup> Dept. of Physiology, University of Granada, Cartuja Campus, 18071 Granada, Spain

<sup>d</sup> Dept. of Parasitology, University of Granada, Avda. Severo Ochoa s/n, 18071 Granada, Spain

### ARTICLE INFO

#### Keywords:

Zinc  
7-Amino-5-methyl-1,2,4-triazolo[1,5-*a*]  
pyrimidine ligand  
Luminescence  
Diabetes  
Lesihmaniiasis  
Chagas

### ABSTRACT

We report on the formation of a triazolopyrimidine derivative ligand, 7-amino-5-methyl-1,2,4-triazolo[1,5-*a*]pyrimidine (7-amtp), and a new family of coordination compounds based on this ligand and zinc as metal ion, synthesized by conventional routes. These materials possess different mononuclear structures, namely [ZnCl<sub>2</sub>(7-amtp)<sub>2</sub>] (1), [Zn(7-amtp)<sub>2</sub>(H<sub>2</sub>O)<sub>4</sub>](NO<sub>3</sub>)<sub>2</sub>·2(7-amtp)·6H<sub>2</sub>O (2) and [Zn(7-amtp)<sub>2</sub>(H<sub>2</sub>O)<sub>4</sub>](SO<sub>4</sub>)·1.5H<sub>2</sub>O (3) derived from the use of different zinc (II) salts, in such a way that the counterions govern the crystallization to a large extent. These compounds present and show variable luminescent properties based on ligand-centred charge transfers which have been deeply studied by Time Dependent Density Functional Theory (TD-DFT) calculations. When these compounds are transferred to solution, preserving complex entities as corroborated by NMR studies, they present interesting anti-diabetic and anti-parasitic capabilities, with a comparatively higher selectivity index than other previously reported triazolopyrimidine-based materials. The results derived from *in vivo* experiments conducted in mice also confirm their promising activity as anti-diabetic drug being capable of dropping glucose levels after oral administration. Therefore, these new materials may be considered as excellent candidates to be further investigated in the field of luminescent coordination compounds with biomedical applications.

### 1. Introduction

Diabetes mellitus (DM) is a group of metabolic disorders which raises blood sugar levels over a prolonged period. This disease generates a huge social and economic problem to the world society since DM has become one of the most relevant health issues in the first world countries, with 422 million adults affected all over the world, and more than a half of them living in these countries [1]. For this reason, a great quantity of drugs are used for the treatment of diabetes to control plasma glucose levels and achieve insulin-mimetic effects, in which each class of drug has different mechanisms of action. Unfortunately, common anti-diabetic drugs are associated with several adverse effects, so that the search for new drugs that can fight this disease effectively with minimal side effects is still an ongoing research field [2]. Recent studies aim to develop new

drugs that can be administered orally for the treatment of diabetes, most of them based on organic compounds [3–5]. As an alternative to this type of materials, coordination compounds have shown promising activity as hypoglycaemic agents for the pharmacotherapy of diabetes [6–7]. Among them, compounds containing Zn (Zn<sup>2+</sup>) have been investigated on recent studies using animal models. In particular, some clinical reports strongly support the thought that Zn<sup>2+</sup> deficiency occurs in diabetic conditions, suggesting that Zn<sup>2+</sup> supplementation will benefit or correct the diabetes-induced Zn<sup>2+</sup> status [8–9]. This cation plays essential structural roles in many proteins and enzymes but also has shown insulin enhancing activity *in vivo* [10]. Considering the different families of Zn<sup>2+</sup> compounds synthesized and found in literature, it may be envisaged that mononuclear Zn<sup>2+</sup> coordination compounds could present interesting anti-diabetic properties [11–25].

\* Corresponding authors.

E-mail addresses: [crissg@ugr.es](mailto:crissg@ugr.es) (C. Sánchez-González), [mquiros@ugr.es](mailto:mquiros@ugr.es) (M. Quirós), [antonio5@ugr.es](mailto:antonio5@ugr.es) (A. Rodríguez-Diéguez).

As expected, a delicate rational design of the organic ligand to be coordinated to the central cation plays a key role. In this line, several ligands containing N atoms have demonstrated to be excellent and versatile building blocks that, with the appropriate charge and multi-connectivity patterns, produce, under conventional routes, multi-dimensional coordination compounds with fascinating physical properties. In this respect, we previously reported the synthesis, structural characterization and anti-diabetic evaluation of multidimensional coordination compounds composed of this kind of ligands [26] and zinc and vanadium ions. Of particular interest is the fact that the metal-organic hybrid nature of these materials offers potentially limitless arrangement types and topological architectures [27–28], reinforcing their versatility of use.

In the last ten years, we and others have reported the use of different triazolopyrimidine derivative ligands with specific antiparasitic activities, with a particular focus on the behaviour of the adenine-derivative 7-amino-1,2,4-triazolo[1,5-*a*]pyrimidine ligand (7-atp) [29–37]. Based on these previous results, a new amine derivative triazolopyrimidine ligand (7-amino-5-methyl[1,2,4]triazolo[1,5-*a*]pyrimidine; 7-amtp hereafter) is designed and synthesized in this work (Scheme I). Additionally, three coordination compounds based on 7-amtp ligand and Zn<sup>2+</sup> are synthesized and characterized, and their anti-diabetic activity evaluated. In this line, it is worth it to mention that the antidiabetic properties of triazolopyrimidine-derivative ligands have been previously reported [38–42] but, to the best of our knowledge, this is the first time where a potential anti-diabetic compound merges the biological activity of this type of ligands with the insulin enhancing activity of the Zn<sup>2+</sup> cation. (See Scheme II.)

Equally important is the fact that, due to its extended aromaticity and to the presence of several heteroatoms in the ring, this ligand should be a good candidate to show luminescent properties, which might be enhanced when coordinated to Zn<sup>2+</sup> ions [43–45]. In this sense, coordination compounds containing metal ions with closed shell configuration, such as d<sup>10</sup> metals (Zn<sup>2+</sup> and Cd<sup>2+</sup>) have attracted extensive interest in recent decades, given their ability to render fascinating structures [46–51]. This fact is a consequence of the absence of ligand field constraints, associated with the d<sup>10</sup> configuration of these ions, which provides flexible coordination environments that can be adapted to a wide variety of geometries. Hence, they allow fine tuning of the structures and/or topologies. Moreover, the closed-shell configuration also possesses some additional advantages regarding the photoluminescence (PL) properties [52–53], since the absence of potential quenching processes derived from *d-d* transitions permits efficient luminescent emission. This fact should allow us to develop multifunctional materials with interesting luminescent and biological properties.

Therefore, we report herein the synthesis and characterization of a

new family of Zn<sup>2+</sup> coordination complexes based on the novel triazolopyrimidine derivative 7-amtp ligand, [ZnCl<sub>2</sub>(7-amtp)<sub>2</sub>] (1), [Zn(7-amtp)<sub>2</sub>(H<sub>2</sub>O)<sub>4</sub>](NO<sub>3</sub>)<sub>2</sub>·2(7-amtp)·6H<sub>2</sub>O (2) and [Zn(7-amtp)<sub>2</sub>(H<sub>2</sub>O)<sub>4</sub>](SO<sub>4</sub>)·1.5H<sub>2</sub>O (3). 1–3 compounds are mononuclear entities in which 7-amtp coordinates via N3 atom (see Scheme I for atom numbering) to zinc ions. Luminescent measurements of compounds have been performed along in vitro anti-parasitic activities and in vivo anti-diabetic properties have been studied in the diabetic murine model STZ-CD1, constituting, to the best of our knowledge, the first report on Zn-based compounds as glucose lowering agents.

## 2. Results and discussion

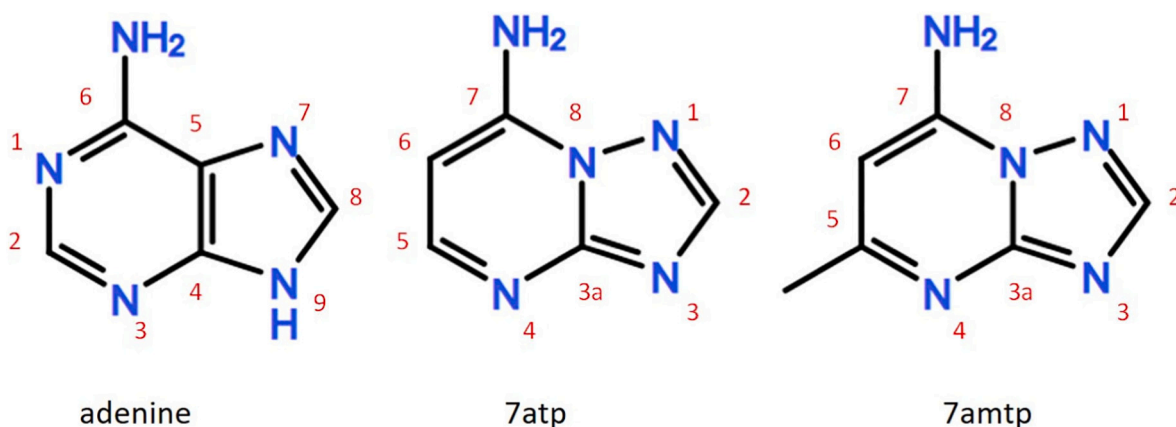
### 2.1. Description of the structures

#### 2.1.1. (7-amtp)·(H<sub>2</sub>O)

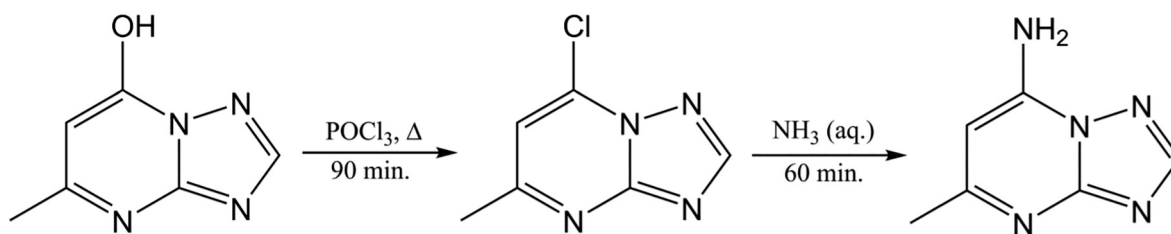
The free 7-amtp ligand crystallizes in the orthorhombic *Pbca* space group with two crystallographically independent molecules in the asymmetric unit, which also contains two crystallization water molecules, one of them disordered between two positions. The crystal architecture is mainly built by hydrogen bonds with water molecules interacting between them (O...O distance, 2.648(3)/2.756(3) Å) and acting as donor towards N3 and N4 atoms of the organic moiety (O...N distances, 2.827(3)/2.850(3), 2.880(2) and 2.820(2) Å, see Fig. 1). The amino groups also act as H-bond donors towards one of the water molecules (N...O distance, 2.746(3)/2.784(3) Å) and to N1 and N3 atoms of neighbouring heterocycles (N...N distances, 2.876(2) and 3.009(2) Å). The planar aromatic moieties stack along the *b* axis (distance ~3.35 Å), each stack being built by symmetry equivalent molecules, related by the *b* glide plane perpendicular to the *a* axis (Fig. S20). Viewed from this direction, the two stacks alternate in a zig-zag-like fashion along the *c* axis.

#### 2.1.2. [ZnCl<sub>2</sub>(7-amtp)<sub>2</sub>] (1)

Compound 1 crystallizes in monoclinic *P2<sub>1</sub>/c* space group, the asymmetric unit being built by just one tetrahedral coordination entity (Fig. 2). Bond lengths and angles are listed in the supplementary material (Table S1). The tetrahedral coordination polyhedron involves two chloride ions and two 7-amtp ligands coordinated to the metallic cation through N3 nitrogen atom of the ring, which is the most usual coordination mode of these kind of ligands. The corresponding bond distances are 2.2395(5) and 2.2934(5) Å (Zn–Cl) and 2.015(2) and 2.021(2) Å (Zn–N3). These units join to one another through hydrogen bonding interactions between chlorine atoms of one complex and amino groups of 7-amtp from neighbouring units (N...Cl distances, 3.344(2), 3.233(2) and 3.280(2) Å). The complexes are associated in centrosymmetric couples via by  $\pi$ -stacking interaction (Fig. S21).



**Scheme I.** Chemical structure of adenine, as well as 7-atp and 7-amtp ligands. Biochemical and IUPAC ring-numbering system has been employed for purine and 1,2,4-triazolo[1,5-*a*]pyrimidine ligands, respectively.



Scheme II. Synthesis procedure for 7-amp.

### 2.1.3. $[\text{Zn}(\text{7-amp})_2(\text{H}_2\text{O})_4](\text{NO}_3)_2 \cdot 2(\text{7-amp}) \cdot 6 \text{H}_2\text{O}$ (**2**)

Compound **2** crystallizes in the triclinic *P*-1 space group. The moieties present in the structure are shown in Fig. 3. Selected bond lengths and angles are given in Table S2. The coordination entity of this compound consists of a zinc cation located on an inversion centre, displaying an octahedral coordination sphere with four water molecules in the equatorial plane and two 7-amp ligands coordinated through N3 nitrogen atoms occupying the positions of the reference axis; the N4 atom of this ligand accepts an H-bond from one of the coordinated water molecules (O1W...N4A distance, 2.713(2) Å) closing a 6-member pseudo-chelating ring. The bond distances in zinc coordination sphere are 2.1471(14) Å for the organic ligand and 2.0650(13) and 2.1830(13) Å for the water molecules. Another molecule of 7-amp is present in the second coordination sphere, interacting with that linked to the metal by  $\pi$  stacking, with alternating coordinated and non-coordinated 7-amp moieties stacked along the *b* axis. The asymmetric unit is completed by one nitrate ion that counterbalances the positive charge of zinc and three non-coordinated water molecules. The later are assembled in centrosymmetric groups of six molecules, with a R4(1) ring and two pending molecules (Fig. S22), which are further linked to the coordinated water molecules and to the anions. Likewise, the amino groups of both ligands also act as H-bond donors towards the groups of six interstitial water molecules and towards the N1 atom of the non-coordinated 7-amp.

### 2.1.4. $[\text{Zn}(\text{7-amp})_2(\text{H}_2\text{O})_4](\text{SO}_4) \cdot 1.5\text{H}_2\text{O}$ (**3**)

Compound **3** crystallizes in triclinic *P*-1 space group. There are two crystallographically independent but chemically equivalent  $[\text{Zn}(\text{7-amp})_2(\text{H}_2\text{O})_4]^{2+}$  cations, both placed on inversion centres and displaying very similar fragments to that described for compound **2**: a zinc cation coordinated to two N3-coordinated 7-amp ligands in the reference axis and four water molecules coordinated in the plane perpendicular to the reference axis. One of the cations is disordered between two positions, one of them is rotated  $\sim 30^\circ$  around the N–Zn–N axis from the other, the disorder thus affecting the coordinated water molecules. A sulphate anion balancing the charge and two crystallization water molecules (one of them with half occupancy close to an inversion centre) complete the structure, a view of the moieties being depicted in Fig. 4. Bond distances in the coordination entity range from 2.08 to 2.15 Å for Zn–O bonds whereas Zn–N distances are 2.145(2) and 2.208(2) Å. The supramolecular structure is governed by hydrogen bond interactions, with a complex network further complicated by the disorder in both coordinated and non-coordinated water molecules. The disordered complex shows a pseudo-chelating ring analogous to that described for compound **2** whereas, for the other one, the interaction is indirect through a non-coordinated water molecule (coordinated  $\text{H}_2\text{O} \dots$  non-coordinated  $\text{H}_2\text{O} \dots \text{N4}$ ). A noteworthy interaction is that taking place between 7-amp moieties related by inversion centres and involving two  $\text{NH}_2 \dots \text{N1}$  H-bonds (N...N distances, 3.022(3) Å for ligand A

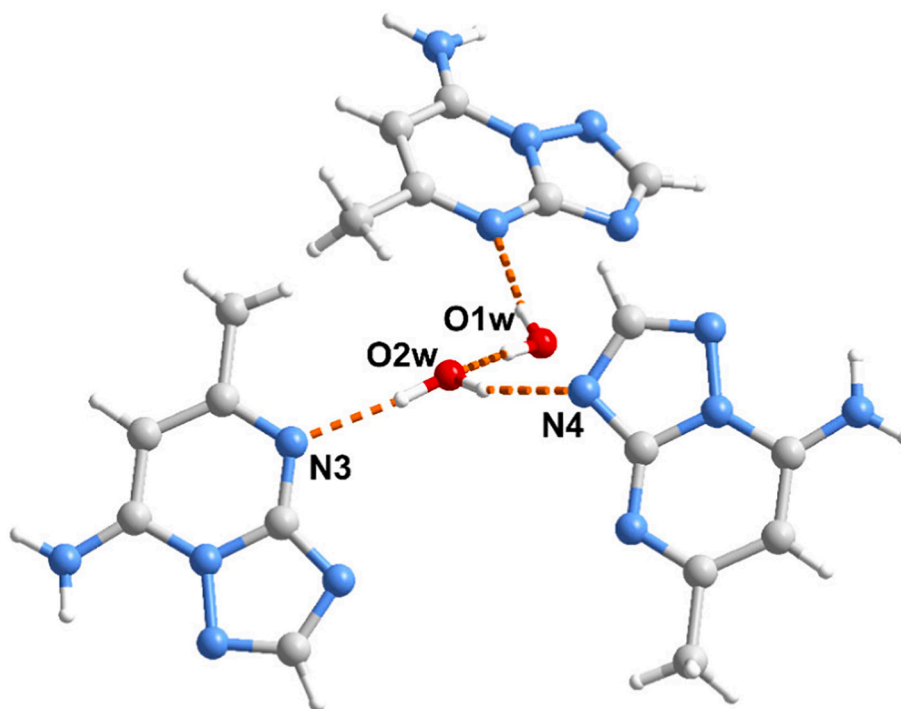
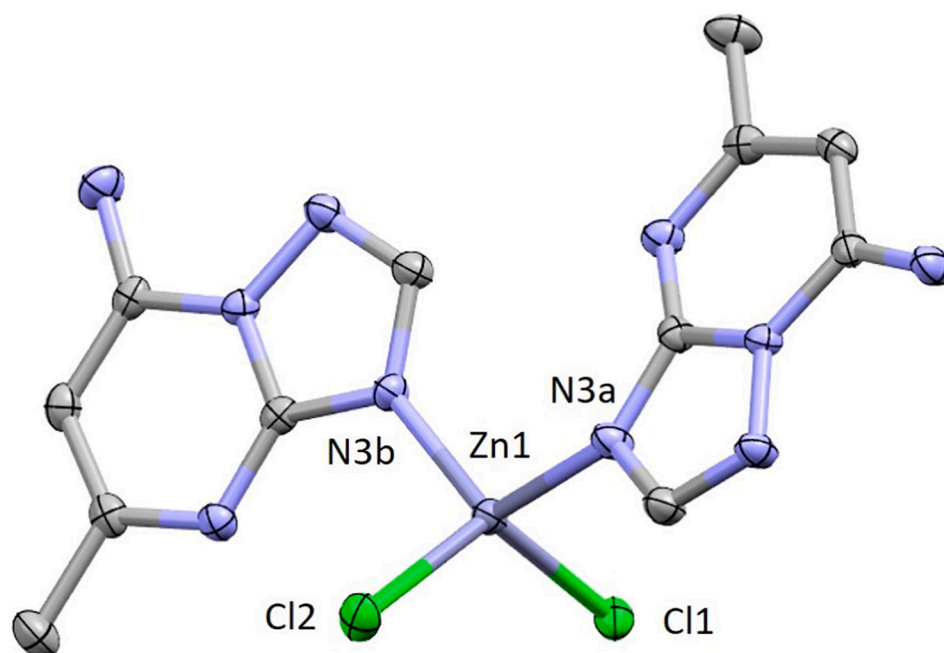
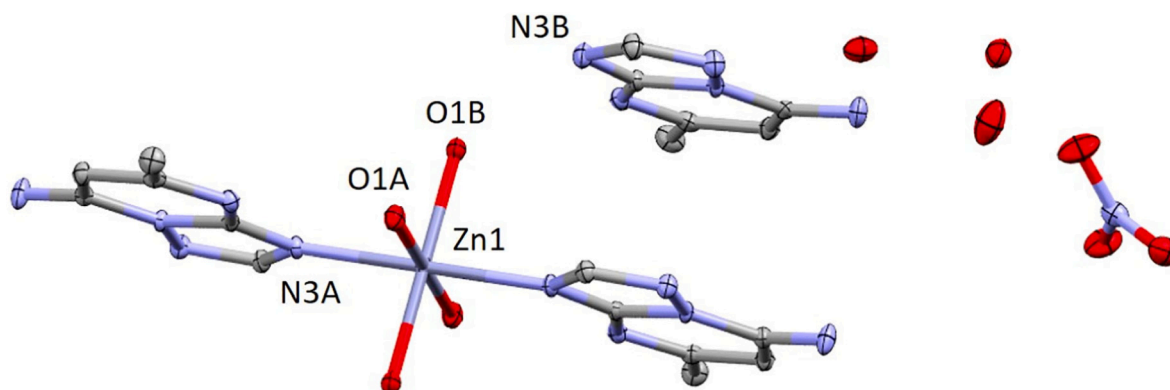


Fig. 1. Fragment of the crystal structure of 7-amp ligand showing most relevant hydrogen bonding interactions. Colour code: carbon, grey; hydrogen, white; nitrogen, blue; oxygen, red. (For interpretation of the references to colour in this figure legend, the reader is referred to the web version of this article.)



**Fig. 2.** Perspective view of mononuclear coordination compound 1. Hydrogen atoms have been omitted for clarity. Colour code: Zinc, light steel blue; nitrogen, blue; carbon, grey; chlorine, green. (For interpretation of the references to colour in this figure legend, the reader is referred to the web version of this article.)



**Fig. 3.** Perspective view of compound 2. Hydrogen atoms have been omitted for clarity. Colour code: zinc, light steel blue; oxygen, red; nitrogen, blue; carbon, grey. (For interpretation of the references to colour in this figure legend, the reader is referred to the web version of this article.)

and 2.951(3) Å for ligand B) this interaction links the complex cations forming rows in the [001] and [011] directions. The anions are also involved in the H-bond network, acting as acceptors for water molecules and amino groups. All organic moieties are roughly perpendicular to the 110 direction but no  $\pi$ -stacking interactions are clearly defined.

## 2.2. NMR studies

In order to determine the purity of the synthesized ligand and whether the crystallized complexes are representative for the sample in solution,  $^1\text{H}$  and  $^{13}\text{C}$  NMR studies were carried. The results of these assays are shown in the figures below.

Fig. 5 shows the  $^1\text{H}$  NMR spectrum for the 7-amtp ligand, carried out in deuterated methanol. Three signals, apart from the two corresponding to the solvent ( $\delta_{\text{CHD}_2} = 3.32$  ppm and  $\delta_{\text{OH}} = 4.86$  ppm) that acts as internal patron, are shown. The signals correspond to the methyl group ( $\delta_{\text{CH}_3} = 2.49$  ppm), C6 carbon ( $\delta_{\text{C}_6} = 6.28$  ppm) and C2 carbon ( $\delta_{\text{C}_2} = 8.29$  ppm). The amino group signal does not appear because its protons are involved in hydrogen bonding interactions and switch with the solvent.

The  $^{13}\text{C}$  NMR spectrum is shown in Fig. 6. It shows six different

signals, apart from the one corresponding to the methanol ( $\delta_{\text{MeOD}} = 47.38$  ppm, which acts again as internal patron:  $\delta_{\text{CH}_3} = 22.97$  ppm,  $\delta_{\text{C}_6} = 90.32$ ,  $\delta_{\text{C}_7} = 149.32$ ,  $\delta_{\text{C}_{3a}} = 153.58$ ,  $\delta_{\text{C}_2} = 155.26$  and  $\delta_{\text{C}_5} = 164.49$  ppm).

The results, which only show the expected signals, confirm the purity of the samples.

## 2.3. Stability studies

To determine the stability of the complexes,  $^1\text{H}$  NMR spectra (Figs. S12–S19) have been recorded for free 7-amtp and the zinc complexes using the culture medium of the parasites and 10%  $\text{D}_2\text{O}$  as solvent to check the stability of the compounds in solution. All spectra have been recorded twice: i) just after the preparation of the solutions and ii) after 72 h, which corresponds to the longest time that the compounds remain in the solution for biological studies.

The free ligand spectra show the expected three signals corresponding to the methyl group ( $\delta_{\text{CH}_3} = 2.32$  ppm), C6 carbon ( $\delta_{\text{C}_6} = 6.17$  ppm) and C2 carbon ( $\delta_{\text{C}_2} = 8.21$  ppm) and the signal of the solvent ( $\delta = 4.70$  ppm) that acts as internal patron. The spectrum remains practically identical after 72 h.

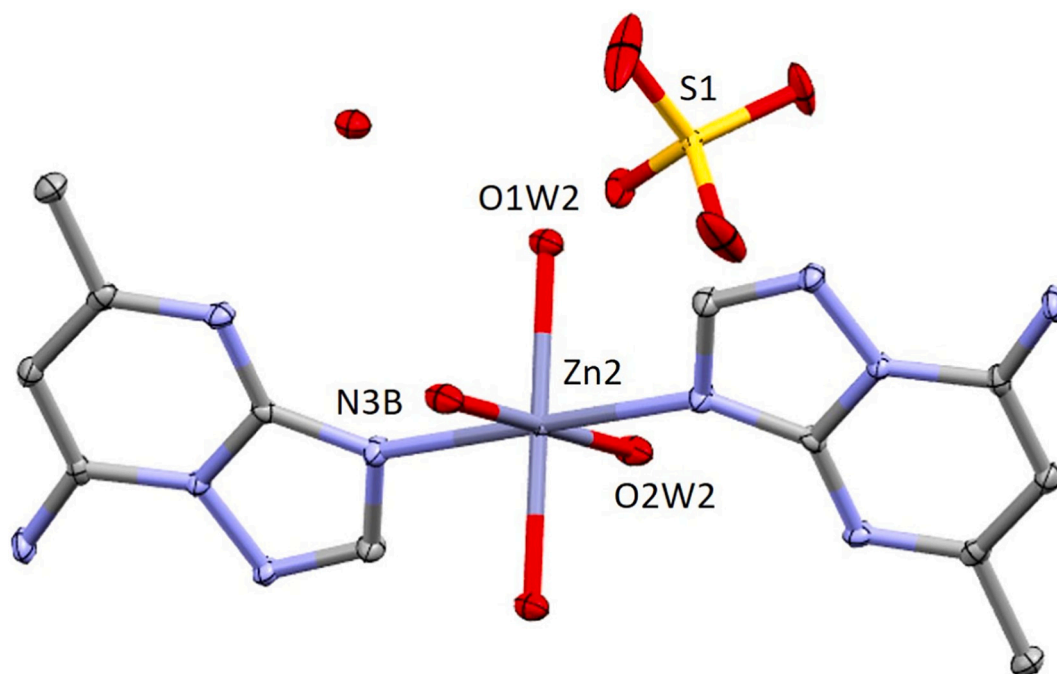


**Fig. 4.** Perspective view of compound 3. Hydrogen atoms have been omitted for clarity. Colour code: zinc, light steel blue; oxygen, red; nitrogen, blue; carbon, grey; sulphur, yellow. (For interpretation of the references to colour in this figure legend, the reader is referred to the web version of this article.)

In the case of compound 1, the three peaks are slightly shifted with respect to the free ligand ( $\delta_{\text{CH}_3} = 2.38$  ppm), C6 carbon ( $\delta_{\text{C}_6} = 6.29$  ppm) and the C2 carbon signal is now divided in two

signals ( $\delta_{\text{C}_2} = 8.25$  and 8.37 ppm), and remains unaltered after 72 h. Regarding compounds 2 and 3, both compounds present very similar spectra, that are practically identical to the free 7-amtp, except for the

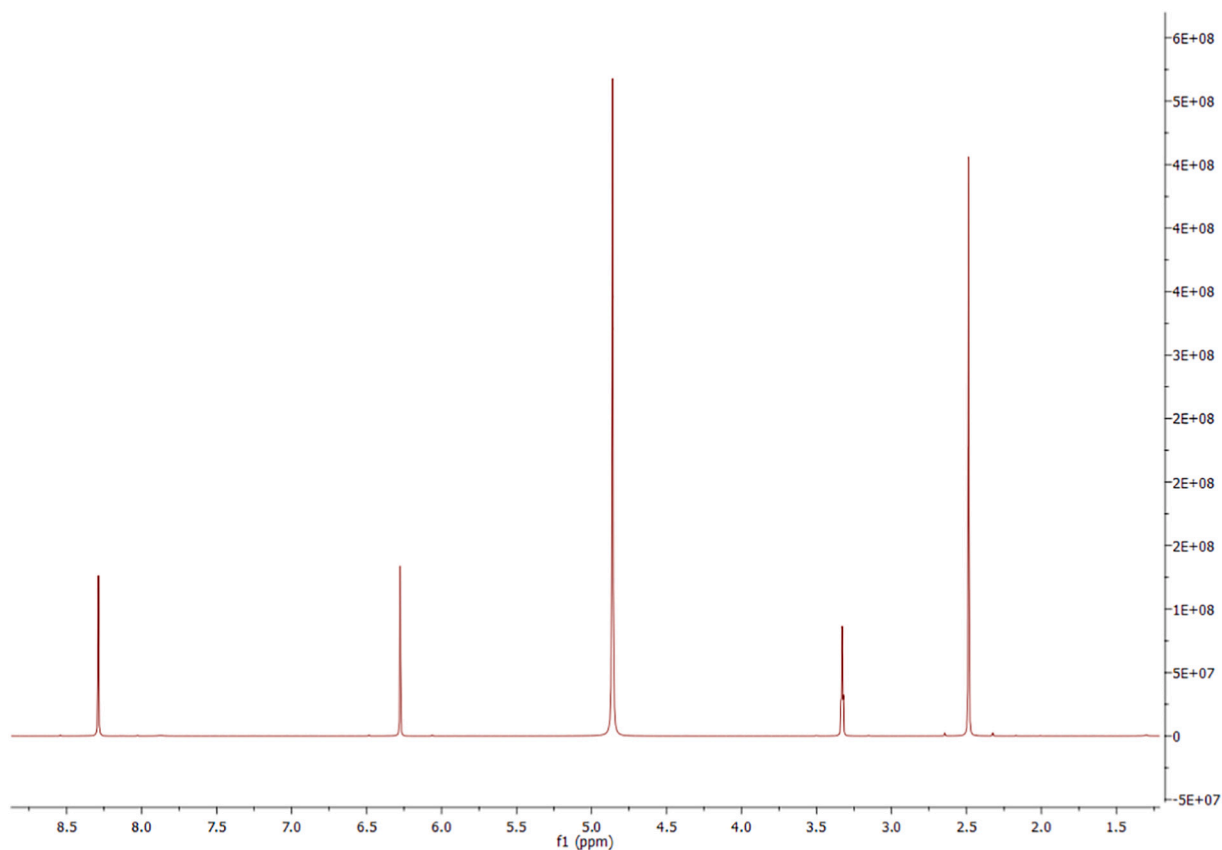


**Fig. 5.**  $^1\text{H}$  NMR spectrum for 7-amtp.

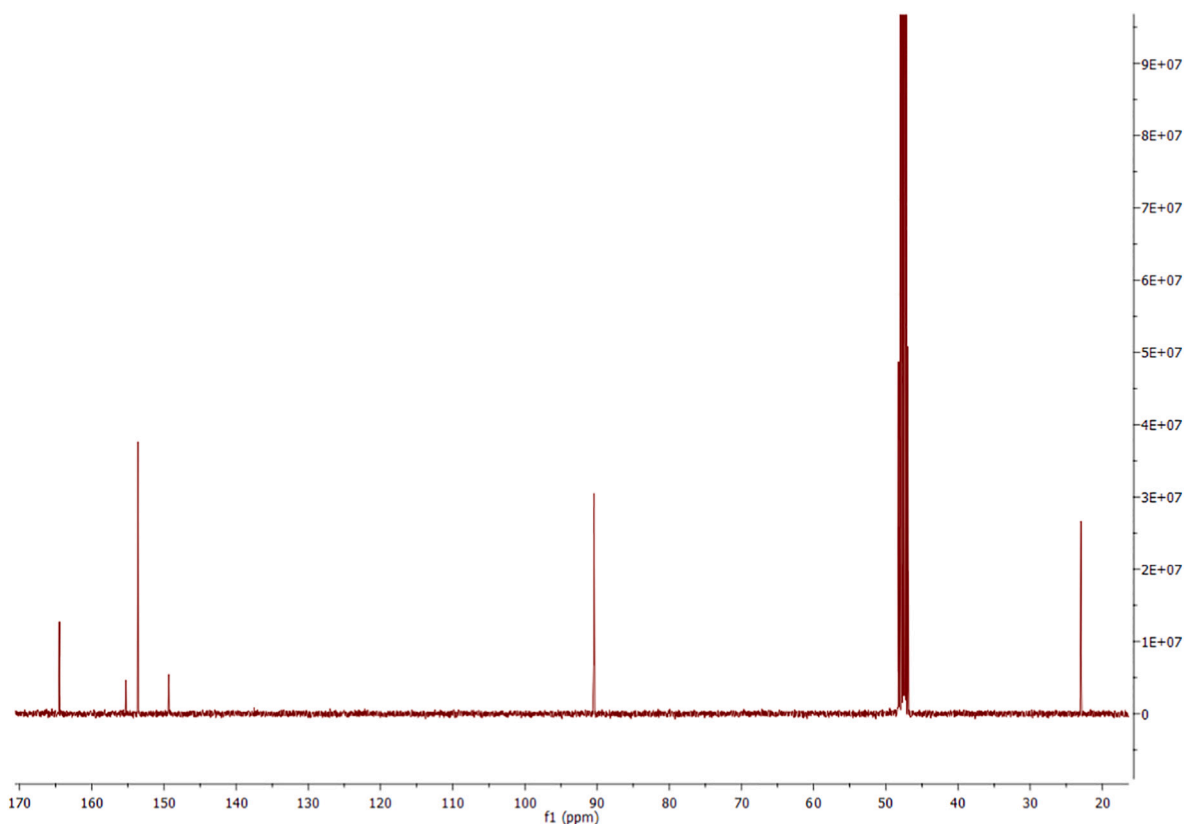


Fig. 6.  $^{13}\text{C}$  NMR spectrum for 7-amtp.

presence of a new peak centred at 7.32 ppm in compound 2 and 7.36 ppm in compound 3. As in the other cases, both spectra remain practically unaltered after 72 h in solution.

Those results suggest that, even if there is a dissociation equilibrium in aqueous solution, all compounds remain, at least, their complex identity (which makes them suitable for biological assays in that kind of media).

#### 2.4. Photoluminescence studies

Solid state photoluminescence measurements were performed on polycrystalline samples of compounds 1–3 and free 7-amtp ligand with the aim of getting a representative characterization of the emissive

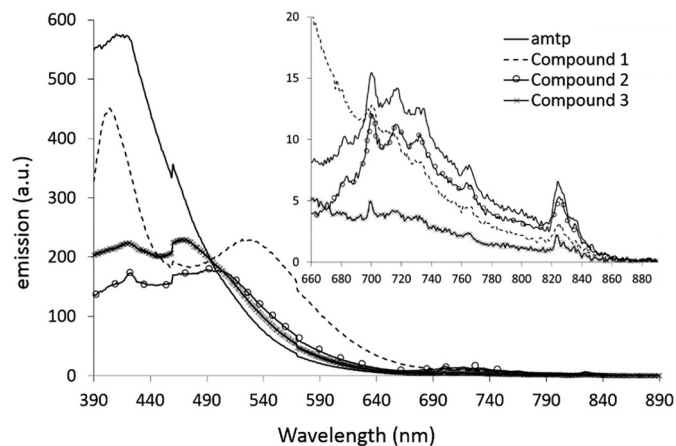
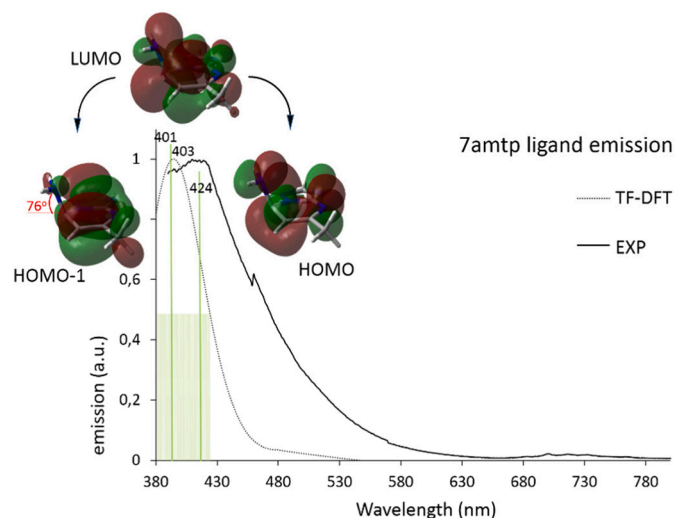


Fig. 7. Room temperature solid state emission spectra of 7-amtp (solid line), compound 1 (dashed line), 2 (circles) and 3 (crosses) upon sample excitation at  $\lambda_{\text{ex}} = 308$  nm.

performance of these compounds to evaluate their potential applications on biomedicine. The emission spectra of 7-amtp and 1–3 at room temperature are shown in Fig. 7. Free 7-amtp ligand shows an intense emission band, centred at about 418 nm, and a much weaker band at around 720 nm, upon excitation at  $\lambda = 308$  nm. The emission spectrum of mononuclear compound 1 shows a weak displacement in the first band, centred at 406 nm, and also reveals a new and less intense band centred at ca. 540 nm. Interestingly, the PL behaviour of compounds 2 and 3 (though similar to each other) differ substantially from that of 1. In this line, the intensity of the more energetic band, centred now at ca. 410 nm, drops substantially and the less energetic band is now equally significant. The latter band, centred at ca. 480 nm and 490 nm respectively for 2 and 3, is therefore significantly blue-shifted with respect to the equivalent signal of compound by 1.

The PL emission properties of these type of complexes is commonly assigned to intraligand  $\pi \leftarrow \pi^*$  electronic transitions. This may be checked by means of Time Dependent Density Functional Theory (TD-DFT) calculations. TD-DFT calculated emission spectrum of the free 7-amtp and the graphical representation of the molecular orbitals (MO) involved in the emission process are shown in Fig. 8, where the main band computed at 403 nm arises from electronic relaxation processes occurring between two sets of molecular orbitals of mixed-nature and centred all over the ligand scaffold. In this sense, the large green vertical lines at 401 and 424 nm, together with the vibrationally related and signal overlapping shorter green vertical lines, represent the energy of the most relevant electronic transitions occurring between the first computed excited singlet-state  $S_1$  and the ground  $S_0$  state. Represented MOs indicate that the promoted electron finally drops from the lowest unoccupied molecular orbital (LUMO) to both the highest occupied molecular orbital (HOMO) (424 nm) as well as to the HOMO-1 (401 nm). Additional data on the computed electronic transitions are collected in Table 1. Interestingly, as observed in the optimized  $S_1$  singlet state excited geometry of 7amtp represented in Fig. 8, an evident



**Fig. 8.** Experimental (solid line) and TD-DFT computed (dashed line) emission spectrum of 7-amp. Green vertical lines identify the computed main transitions responsible for the corresponding maximum (see Table 1). (For interpretation of the references to colour in this figure legend, the reader is referred to the web version of this article.)

**Table 1**

Major electronic transitions computed to be responsible for the emission spectra of 7-amp, **1** and **2**.

	Emiss. (nm)	Main trans.	Symm.	Osc. st
7-amp	401	H-1 $\leftarrow$ L (90%)	Singlet	0.0634
	424	H $\leftarrow$ L (95%)	Singlet	0.0579
<b>1</b>	386	H-1 $\leftarrow$ L (91%)	Singlet	0.0012
	448	H-1 $\leftarrow$ L (90%)	Singlet	0.0011
	532	H-1 $\leftarrow$ L + 4 (90%)	Singlet	0.0065
	589	H-1 $\leftarrow$ L + 3 (90%)	Singlet	0.0051
<b>2</b>	479	H $\leftarrow$ L + 23 (90%)	Singlet	0.0452
	509	H $\leftarrow$ L + 21 (95%)	Singlet	0.0419

out-of-plane twist of the amine substituent is forced upon electron absorption and subsequent vibrational relaxation of the ligand, yielding an  $S_1$  excited state where the N atom of the amine substituent is positioned up to  $76^\circ$  out of the plane generated by the aromatic portion of the ligand. Notwithstanding the fact that the use of no geometrical constraints in the emission calculations may permit larger conformational adjustments in the molecules than the ones permitted in a closely packed crystal of 7amp, the mentioned twist might still occur in the sample, though its extent is difficult to measure.

The same type of calculations carried out on **1** yielded the computational emission spectrum shown in Fig. 9a (dashed line), which is, again, in very good agreement with the experimental data.

Characterized by one wide band centred at ca. 381 nm, and a weaker one at ca. 566 nm, both computed bands actually result from electron relaxation processes occurring from two distinct but energetically low-lying singlet excited states,  $S_1$  and  $S_2$ . The former excited state geometry reveals a significant out-of-plane twist of the amine group in 7amp, resembling  $S_1$  in the free 7amp ligand, whereas the latter ( $S_2$ ) does not. As derived from the diagrams shown in Fig. 9b, the more energetic emission can be described as a ligand-to-ligand charge transfer (LLCT) process happening in the thermally relaxed  $S_1$  species, and can be ascribed to an electron decay from a 7-amp ligand centred large LUMO orbital to the as well 7-amp ligand centred HOMO-1 molecular orbital. The less energetic emission band, also a LLCT photoluminescent process, differs substantially from the one just described, as the HOMO-1 molecular orbital receiving the relaxing electron was computed to be centred in the chloride ligand (presumably 3p atomic

orbital). Electrons reach the latter orbital upon undergoing an emissive relaxation from the 7-amp-ligand centred LUMO + 3 and LUMO + 4 molecular orbitals, respectively. Both MOs are involved in the two major contributions identified in this region. In this sense, the H-1  $\leftarrow$  L + 3 transition is responsible for the 532 nm line, whereas the 589 nm line arises from an H-1  $\leftarrow$  L + 4 electronic relaxation process.

Computed emission spectrum of **2** (Fig. 9c), again in very good agreement with the experimental data, revealed a single and rather wide maximum centred at ca. 453 nm, followed by a slowly decaying shoulder centred in ca. 489 nm. Both signals arise from two major transitions at 479 nm and 509 nm (green and blue vertical large lines, see Table 1), respectively, as well as from multiple vibrationally related less significant transitions (shorter green and blue vertical lines). As indicated in the diagram depicted Fig. 9d, the observed PL behaviour is understood on the basis of a complex inter-ligand electronic relaxation process occurring between the LUMO + 21 and the HOMO; on the contrary, the mentioned shoulder at ca. 489 nm is actually derived from a major electronic transition occurring at 509 nm (large blue vertical line in Fig. 9c) as well as the related vibrational levels (shorter blue vertical lines). These electronic transitions have a complex origin, since both metal and ligand contributions are observed in the LUMO + 23 identified as the one releasing the electrons responsible for the mentioned emission shoulder.

## 2.5. Anti-parasitic assays

7-amp derivative and three obtained zinc (II) complexes were assayed against extracellular forms of *L. infantum*, *L. braziliensis* and *T. cruzi*. Additionally, cytotoxicity studies were carried out over macrophages and Vero cells, which are host cells for *Leishmania* spp. and *T. cruzi*, respectively. The results of in vitro assays are shown in Table 2.

The 7-amp derivative shows a quite similar antiproliferative activity compared to the observed for all previously studied triazolopyrimidine derivatives [54], with **1** that are a little better than the values for the reference drugs. On the other hand, we can see that all compounds show a remarkable activity against all parasites, especially compound **1** against *L. braziliensis* and compound **2** against *T. cruzi*, whose  $IC_{50}$  values are below the lowest concentration studied. Additionally, all compounds show a cytotoxicity that is a magnitude order higher than reference drugs. This fact united to the great antiproliferative activity results on high selectivity indexes, which are 6 times better than reference drugs in the less effective situations and more than three hundred in the best assays. Additionally, all compounds present SI values that are rather higher than the obtained for similar zinc compound previously obtained [55,56]. These data show that all compounds and especially compound **1** are promising prodrugs to continue studying them in further in vitro and in vivo assays to conclude their potential use as antiparasitic therapeutic agents.

## 2.6. In vivo assays

The essays were performed in STZ-CD1 mice with severe hyperglycaemia induced as indicated in the experimental section. The test of the oral glucose tolerance (Fig. 10) showed different types of hypoglycaemic effects exerted by the above characterized Zn compounds. Compound **1** did not avoid the increase of the glycaemic peak 30 min after glucose oral administration, but reduced significantly glycaemia after 60 min in comparison with untreated diabetic mice, and achieved the normalization of blood glucose levels, approaching the glucose levels to that found in healthy mice at the end of the test. Compound **2** yielded the best anti-diabetic properties of the three compounds, because mice treated with compound **2** maintained the lower blood glucose levels during all the test. 30 min after glucose oral administration mice treated with compound **2** showed glucose levels statistically equal to healthy mice. On the other hand, compound **3** exhibited a blood glucose lowering effect consisting in preventing the glycaemic peak

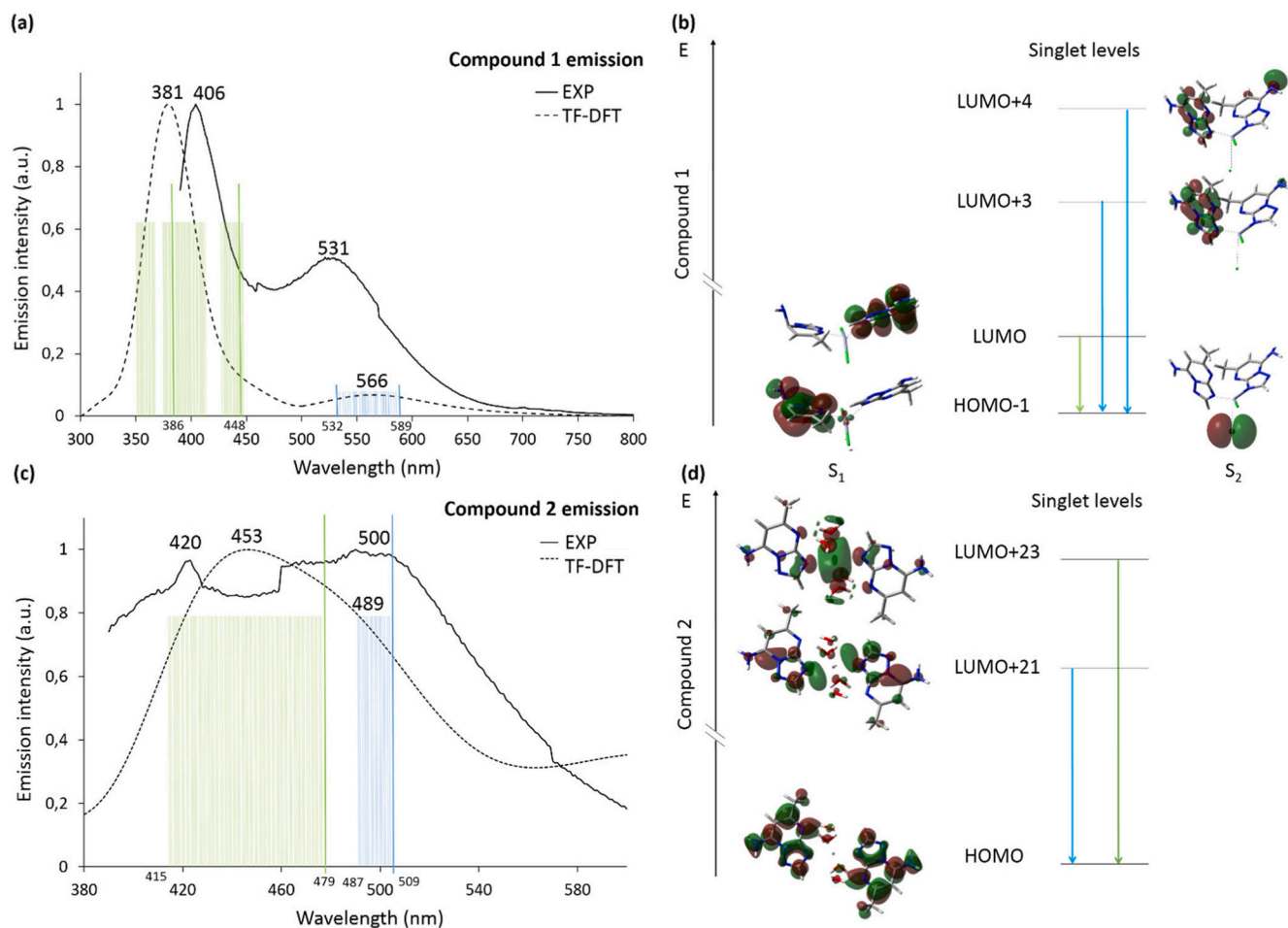


**Fig. 9.** Experimental (solid line) and computed (dashed line) emission spectra of compound 1 (a) and 2 (c). Main transitions in the computed spectrum are identified by large vertical green and blue lines, respectively, whereas vibrationally related transitions are depicted by shorted lines; (b) Graphical representation of the MOs in S<sub>1</sub> and S<sub>2</sub> of compound 1 (b) and 2 (d) involved in the main electronic transitions. (For interpretation of the references to colour in this figure legend, the reader is referred to the web version of this article.)

caused by the oral glucose load. However, unlike compounds 1 and 2, compound 3 failed to normalize glucose levels and bring them closer to the levels found in healthy mice. None of those effects is observed for the free ligand that, far from exerting an anti-diabetic effect, exerted a hyperglycaemic effect from the beginning until the end of the test.

The results obtained in vivo in the present study show that the tested compounds display interesting potential as anti-diabetic drugs [57]. Compound 2 shows an interesting effect 30 min after oral glucose overload and manages to reach blood glucose levels of healthy mice,

but does not avoid a glycaemic peak of 37% of the baseline at 15 min. Meanwhile, compound 3 fails to normalize blood glucose at the end of the test, but prevents the trigger effect allowing an increase in glycaemia of only 13%. The synergistic effect of the simultaneous combined administration of the two compounds could cover the two targets: avoid the postprandial glycaemic peak and normalize glucose levels to those of the state of health. Further studies will be needed to better understand the mechanisms underlying the effects of the synthesized compounds.

**Table 2**

In vitro activity of 7-amp and zinc (II) complexes and reference drugs against promastigote forms of *Leishmania spp.*, epimastigote forms of *Trypanosoma cruzi*, J774.2 macrophages and Vero cells after 72 h of incubation at 37 °C.

Compound	IC <sub>50</sub> ± SD (µM) <sup>a</sup>					SI <sup>b</sup>		
	<i>L. inf.</i>	<i>L. brazii.</i>	<i>T. cruzi</i>	Macrophages J774.2	Vero cells	<i>L. inf.</i>	<i>L. brazii.</i>	<i>T. cruzi</i>
Glucantime®	18.0 ± 0.6	25.6 ± 1.6	–	15.2 ± 1.3	–	0.8	0.6	–
Benznidazole®	–	–	24.2 ± 1.9	–	13.6 ± 0.9	–	–	0.9
7-amp	32.9 ± 2.6	13.4 ± 1.1	35.6 ± 2.8	147.9 ± 14.0	394.3 ± 31.5	5.3 (7)	13.1 (22)	11.1 (12)
1	9.0 ± 0.7	< 1	8.4 ± 0.7	218.1 ± 17.4	288.5 ± 23.1	24.3 (30)	> 218.1 (363)	34.3 (38)
2	29.1 ± 2.3	7.5 ± 0.6	< 1	144.7 ± 11.6	302.6 ± 24.2	5.0 (6)	19.4 (32)	> 302.6 (336)
3	20.1 ± 1.6	5.3 ± 0.4	10.4 ± 0.8	179.3 ± 14.3	406.6 ± 32.5	8.9 (11)	33.8 (56)	39.1 (43)

The results presented are averages of three separate determinations.

<sup>a</sup> The concentration required to obtain 50% inhibition, calculated through a linear regression analysis from the Kc values at the concentration employed (1, 10, 25 and 100 µM for promastigote and epimastigote forms of *Leishmania spp.* and *Trypanosoma cruzi* respectively and 50, 100, 200 and 400 µM for host cells).

<sup>b</sup> Selectivity index (SI) = IC<sub>50</sub> against J774.2 macrophages or Vero cells / IC<sub>50</sub> parasite (promastigote or epimastigote forms respectively).

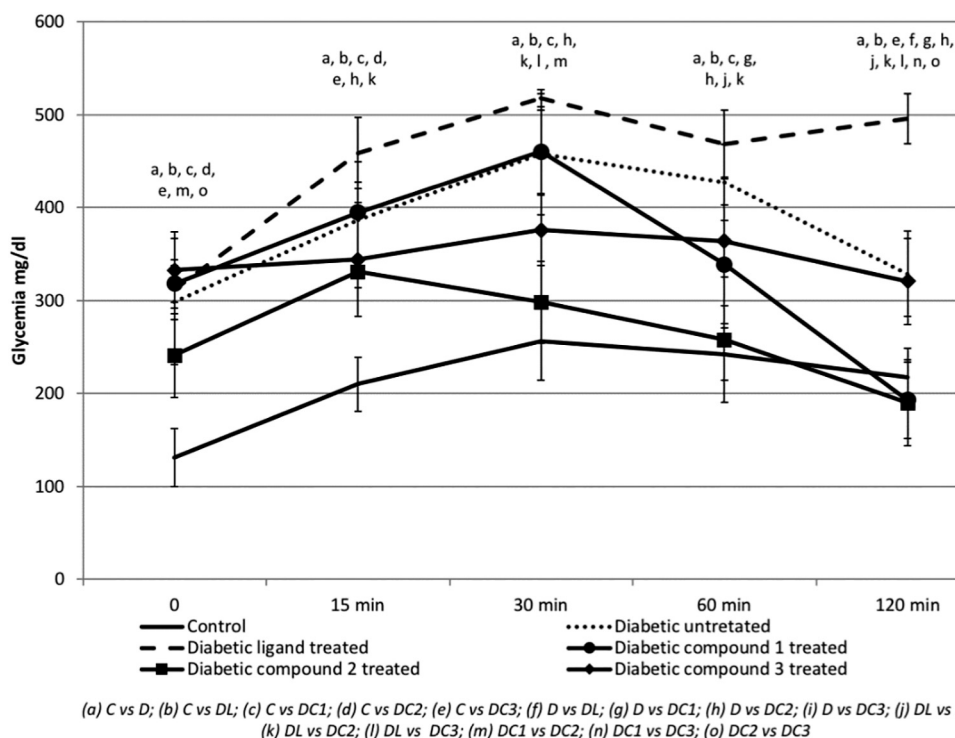


Fig. 10. Oral glucose tolerance test for control (C), diabetic untreated (D), and diabetic mice treated with the ligand (DL) or Zn compound 1 (DC1), 2 (DC2) or 3 (DC3). Data are presented as mean  $\pm$  SD.  $p < 0.05$ .

To the best of our knowledge, this is the first time that Zn-based compounds behaving as glucose lowering agents have been tested in diabetic murine model STZ-CD1, proving that it is an adequate model to validate the effectiveness of new designed drugs. This murine model of low size and body weight presents the advantage of requiring the synthesis of a lower amount of drugs and responds in a sensitive way to the administration of drugs related to hydrocarbon metabolism, this being more versatile than the use of Wistar rats [58–62].

### 2.7. Comparative studies with previous zinc (II) complexes containing 7-atp

Due to the great similarity between 7-atp and 7-amtp, we decided to compare synthesized compounds with the previously reported complexes of zinc (II) containing 7-atp. To our knowledge, three complexes had been previously obtained with the mentioned ligand and ion, containing the auxiliary ligands bipyrimidine (bpym), malonate (mal) and 1,3-propanediamine (tn):  $[\text{Zn}_2(\mu\text{-7-atp})_2(\mu\text{-mal})_2(\text{H}_2\text{O})_2]$  [31],  $[\text{Zn}(\mu\text{-7-atp})(\text{tn})(\text{ClO}_4)]_n$  [36],  $[\text{Zn}_2(7\text{-atp})_4(\mu\text{-bpym})(\text{H}_2\text{O})_4](\text{ClO}_4)_4 \cdot 2(7\text{-atp})$  [56].

Regarding the structure, the three complexes presented in this work are mononuclear and discrete entities, with tetrahedral and octahedral structures, for compounds (1) in the first case and (2) and (3) for the second one. However, the compounds with 7-atp containing bipyrimidine and malonate [31,56] are both dinuclear entities, and the one that contains 1,3-propanediamine [36] forms chains. In fact, only the compound with bpym shows the same coordination way for the ligand, it is monodentate through N3, whereas the others show a bridge mode, through N3 and N4 in the case of the compound with malonate, and through N3 and through N2, N4 and the amino nitrogen in the chain-forming complex. However, the luminescence properties observed in the three compounds, however, are quite similar to the observed for the two compounds that were analysed in that way [31,36].

Zinc compounds have shown effectiveness in the treatment of type 1 and type 2 diabetes by acting at different levels: for their antioxidant properties and acting on numerous intracellular enzymes involved in lipid and glucidic metabolism. Among others, some of the main

proposed mechanisms of action are summarized. Zn compounds have been shown to increase the activity of glycolytic enzymes such as phosphofructokinase (PFK) and pyruvate kinase (PK). Furthermore, in zinc-treated cells a progressive activation of ERK2/MAPK1 (Mitogen-activated protein kinase-1) was observed. Zinc is reversible inhibitor of  $\alpha$ -glucosidase activity in the gut. In skeletal muscles Zinc- $\alpha$ -glycoprotein promotes the phosphorylation of AMP-activated protein kinase (AMPK $\alpha$ ) and increases cellular glucose transporter type 4 (GLUT4) protein. Zinc stimulates the phosphorylation of the IR- $\beta$  (insulin receptor) subunit, and inhibits glycogen synthase kinase-3 (GSK-3 $\beta$ ), which is a phosphorylating and an inactivating agent of glycogen synthase, with resultant increase in glycogen synthesis. Zinc- $\alpha$ -glycoproteins increase the expression of the lipolytic enzymes, adipose triglyceride lipase and hormone-sensitive lipase in the white adipose tissue [63].

### 3. Conclusion

In summary, the novel 7-amino-5-methyl-1,2,4-triazolo[1,5-a]pyrimidine ligand and new family of zinc coordination compounds have been synthesized and characterized by single crystal X-ray diffraction:  $[\text{ZnCl}_2(7\text{-amtp})_2]$  (1),  $[\text{Zn}(7\text{-amtp})_2(\text{H}_2\text{O})_4](\text{NO}_3)_2 \cdot (7\text{-amtp})_2 \cdot 6\text{H}_2\text{O}$  (2) and  $[\text{Zn}(7\text{-amtp})_2(\text{H}_2\text{O})_4]\text{SO}_4 \cdot 1,54\text{H}_2\text{O}$  (3). They are mononuclear compounds in which 7-amino-5-methyl-1,2,4-triazolo[1,5-a]pyrimidine coordinates by N3 atom to zinc ions. Solid state photoluminescence spectra of compounds 1–3 showed the relevance of the excellent luminescence afforded by the 7-amtp ligand, which is modulated according to the conformation acquired in the complex. An exhaustive computational study with TD-DFT theory, permits identifying the molecular orbitals (with high ligand contribution) involved in the excitation and emission, concluding that both first- ( $S_1$ ) and second ( $S_2$ ) excited states take part in the luminescence process. In particular, under excitation with ultraviolet light, all compounds share the occurrence of two bands with blue and green emission, the first of which arises from an intraligand charge transfer whereas the second one has a more complex origin involving a ligand-to-metal charge transfer.

These materials also possess interesting anti-parasitic and anti-diabetic capabilities. On the one hand, all compounds show a remarkable activity against all parasites, especially compound **1** against *L. braziliensis* and compound **2** against *T. cruzi*, whose  $IC_{50}$  values are below the lowest concentration studied. When dissolved in the culture medium of the parasites, the complexes are preserved (though compounds **2** and **3** are partially dissociated) as confirmed by NMR experiments. This fact makes the compounds very suitable for further antiparasitic studies, both in vitro and in vivo, to determine their applicability as drugs. On the other hand, compounds display interesting potential as anti-diabetic drugs due to compound **2** shows an interesting effect 30 min after oral glucose overload and manages to reach blood glucose levels of healthy mice, meanwhile compound **3** fails to normalize blood glucose at the end of the test, but prevents the trigger effect allowing an increase in glycaemia of only 13%. Moreover, to the best of our knowledge, this is the first time that Zn-based compounds behaving as glucose lowering agents have been tested in diabetic murine model STZ-CD1, proving that it is an adequate model to validate the effectiveness of new designed drugs. With all of the above in mind, we have demonstrated the capacity of this new ligand to form coordination compounds, making of them excellent candidates to be further investigated as luminescent probes with biomedical potential applications.

## 4. Experimental section

### 4.1. Materials and physical measurements

All reagents were obtained from commercial sources and used as received. Elemental analyses were carried out at the "Centro de Instrumentación Científica" of the University of Granada on a THERMO SCIENTIFIC analyser model Flash 2000. The IR spectra on powdered samples were recorded with a BRUKER TENSOR 27 FT-IR and OPUS data collection program. The UV spectra in solution were collected on an Agilent Technologies Cary 100 Spectrophotometer. Powder DRX data were collected on a Bruker D2 Phaser diffractometer with monochromated  $CuK\alpha$  radiation ( $\lambda = 1.5405 \text{ \AA}$ ) over the range  $5 < 2\theta < 35^\circ$ . Thermal behaviour (thermogravimetry – TG – and differential scanning calorimetry – DSC) was studied under an air flow in Shimadzu TGA-50 and Shimadzu DSC-50 equipments at heating rates of 20 and  $10 \text{ }^\circ\text{C min}^{-1}$  respectively. NMR spectra were collected with a high definition 500 MHz NMR spectrometer BRUKER Avance NEO using MeOD as solvent. Those used to analyse the stability of the complexes in solution, were carried in the same spectrometer, using medium trypanosome liquid (MTL) + 10%  $D_2O$  as solvent.

### 4.2. Synthesis of 7-amino-5-methyl-[1,2,4]triazolo[1,5-a]pyrimidine (7-amp $H_2O$ )

The triazolopyrimidinic derivative used as a ligand was prepared following the method described by Makisumi [64], in which 29 mmol (0.5 g) of 7-hydroxy-5-methyl-1,2,4-triazolo[1,5-a]pyrimidine (HmtpO) were added on a round flask with 10 mL of phosphoryl chloride and put in reflux for 90 min, while the mixture turned dark orange. After this time, solution is cooled up to room temperature and the mixture is basified with sodium hydrogen carbonate until there was no visible reaction. Then, the solution is extracted with dichloromethane and the chlorated intermediate is collected by using a rotoevaporator. Obtained product (7-chloro-5-methyl-1,2,4-triazolo[1,5-a]pyrimidine) was putted in a excess of commercial ammonia solution and magnetically stirred during an hour. After this time, yellow crystals of amino derivative (7-amp) were obtained, some of them suitable for XRD measures. Yield: 73%, based on HmtpO. Anal. Calcd.  $C_6H_9N_5O$ : C, 43.11; H, 5.43; N, 41.89. Found: C, 43.22; H, 5.39; N, 42.01. IR:  $1483 \text{ cm}^{-1}$  ( $\nu_{N-H(\text{flex})}$ ),  $1573 \text{ cm}^{-1}$  ( $\nu_{py}$ ),  $1660 \text{ cm}^{-1}$  ( $\nu_{tp}$ ),  $3096 \text{ cm}^{-1}$  ( $\nu_{O-H}$ ) and  $3300 \text{ cm}^{-1}$  ( $\nu_{N-H(\text{tens})}$ ).

### 4.3. Synthesis of $[ZnCl_2(7-amp)_2]$ (**1**)

A solution of 2 mmol (0.330 g) of 7-amp in 15 mL of water was prepared with stirring and soft warming. Once the ligand was totally dissolved, a solution of  $ZnCl_2$  (2 mmol, 0.389 g) was added. The resulting solution was left at room temperature. After 48 h, yellow prismatic crystals suitable for XRD measurements appeared and were collected by vacuum filtration. Yield: 84%, based on Zn. Anal. calcd. for  $C_{12}H_{14}N_{10}Cl_2Zn$ : C, 33.16; H, 3.25; N, 32.23. Found: C, 33.12; H, 3.08; N, 32.30%. IR:  $1498$  and  $1597 \text{ cm}^{-1}$  ( $\nu_{N-H(\text{flex})}$ ),  $1562 \text{ cm}^{-1}$  ( $\nu_{py}$ ),  $1645 \text{ cm}^{-1}$  ( $\nu_{tp}$ ),  $3350$  and  $3457 \text{ cm}^{-1}$  ( $\nu_{N-H(\text{tens})}$ ).

### 4.4. Synthesis of $[Zn(7-amp)_2(H_2O)_4](NO_3)_2 \cdot 2(7-amp) \cdot 6H_2O$ (**2**)

A solution of 2 mmol (0.300 g) of 7-amp in 15 mL of water was prepared as previously described. Then, a solution of  $Zn(NO_3)_2$  (2 mmol, 0.415 g) in the same solvent was added to the ligand solution. After 24 h at room temperature, pale yellow prismatic crystals suitable for XRD measurements appeared and were collected by vacuum filtration. Yield: 84%, based on Zn. Anal. calcd. for  $C_{24}H_{48}N_{22}O_{16}Zn$ : C, 29.84; H, 5.01; N, 31.89. Found: C, 29.89; H, 4.92; N, 31.81%. IR:  $1298 \text{ cm}^{-1}$  ( $\nu_{NO_3}$ ),  $1504$  and  $1605 \text{ cm}^{-1}$  ( $\nu_{N-H(\text{flex})}$ ),  $1579 \text{ cm}^{-1}$  ( $\nu_{py}$ ) and  $1639 \text{ cm}^{-1}$  ( $\nu_{tp}$ ).

### 4.5. Synthesis of $[Zn(7-amp)_2(H_2O)_4]SO_4 \cdot 1.5H_2O$ (**3**)

A solution of  $ZnSO_4$  (2 mmol, 0.321 g) in water was added over a solution of 2 mmol (0.296 g) of 7-amp in 15 mL of the same solvent. The solution was left at room temperature during 72 h. Finally, light yellow prismatic crystals suitable for XRD measurements appeared and were collected by vacuum filtration. Yield: 82%, based on Zn. Anal. Calcd. for  $C_{12}H_{25}N_{10}O_{9.5}SZn$ : C, 25.79; H, 4.51; N, 25.06. Found: C, 25.98; H, 4.72; N, 25.12%. IR:  $1090 \text{ cm}^{-1}$  ( $\nu_{SO_4}$ ),  $1495$  and  $1591 \text{ cm}^{-1}$  ( $\nu_{N-H(\text{flex})}$ ),  $1583 \text{ cm}^{-1}$  ( $\nu_{py}$ ) and  $1653 \text{ cm}^{-1}$  ( $\nu_{tp}$ ).

### 4.6. Crystallographic refinement and structure solution

X-ray data collection of suitable single crystals of compounds were done at 100(2) K on a Bruker VENTURE area detector equipped with graphite monochromated Mo-K $\alpha$  radiation ( $\lambda = 0.71073 \text{ \AA}$ ) by applying the  $\omega$ -scan method. The data reduction were performed with the APEX2 [65] software and corrected for absorption using SADABS [66]. Crystal structures were solved by direct methods using the SIR97 program [67] and refined by full-matrix least-squares on  $F^2$  including all reflections using anisotropic displacement parameters by means of the SHELXL program (version 2018/3) [68]. One of the water molecules in the structure of the ligand have been disordered between two equally populated positions. Likewise, the water molecules belonging to one of the complexes in compound **3** have been disordered between two positions with relative occupancies 0.6 and 0.4 and an interstitial water molecule in this compound is also disordered between two nearby positions related by an inversion centre. Hydrogen atoms belonging to the heterocycle were included in ideal positions riding on their parent atoms where those belonging to water molecules were located in Fourier difference maps and refined with fixed O–H distances ( $0.84 \text{ \AA}$ ) with the exception of those belonging to the disordered water molecules in compound **3** that were not located or introduced. An isotropic thermal displacement parameter 1.2 times or 1.5 times those of their parent atoms was used for H-atoms. Details of the structure determination and refinement of compounds are summarized in Table S1. Crystallographic data for the structures reported in this paper have been deposited at the Crystallography Open Database (COD) with reference numbers 3000220-23 and at the Cambridge Crystallographic Data Centre (deposition nos. 1893521–24). The files may be directly downloaded from COD website (<http://www.crystallography.net>) or obtained free of charge on application to the CCDC Director, 12 Union

Road, Cambridge, CB2 1EZ, U.K. (Fax: +44-1223-335033; e-mail: [deposit@ccdc.cam.ac.uk](mailto:deposit@ccdc.cam.ac.uk) or <http://www.ccdc.cam.ac.uk>).

#### 4.7. Luminescence measurement

A Varian Cary-Eclipse fluorescence spectrofluorimeter was used to obtain the fluorescence spectra. The spectrofluorimeter was equipped with a xenon discharge lamp (peak power equivalent to 75 kW), Czerny–Turner monochromators, and an R-928 photomultiplier tube which is red sensitive (even 900 nm) with manual or automatic voltage control using the Cary Eclipse software. The photomultiplier detector voltage was 700 V and the instrument excitation and emission slits were set at 5 and 5 nm, respectively.

#### 4.8. TD-DFT calculations

The PL spectra of complexes **1** and **2** (**3** was omitted due to similarity with **2**) and free 7-amtp ligand were calculated computationally by means of TD-DFT using the Gaussian 09 package [69], using the CAM-Becke three parameter hybrid functional with the non-local correlation functional of Lee-Yang-Parr (B3LYP) [70–72] along with 6-311G++(d,p) basis set [73] was adopted for all atoms but for the central zinc cations. Instead, the LANL2DZ [74–76] basis set along with the corresponding effective core potential (ECP) was used for metal atoms. The latter strategy has proven successful in describing luminescence performance of zinc based coordination compounds [77,78]. The 200 lowest excitation and emission energies were calculated by the TD-DFT method. Results were analysed with GaussSum program package [79] and molecular orbitals plotted using GaussView 5 [80].

#### 4.9. Antiproliferative assays

Promastigote forms of *L. infantum* (MCAN/ES/2001/UCM-10), *L. braziliensis* (MHOM/BR/1975/M2904), and epimastigote forms of *Trypanosoma cruzi* (IRHOD/CO/2008/SN3) were cultivated in vitro in medium trypanosome liquid (MTL) [Hank's Balanced Salt Solution (HBSS) (Gibco), NaHCO<sub>3</sub>, lactalbumin, yeast extract, bovine haemoglobin and antibiotics] with 10% inactive fetal bovine serum and were kept in an air atmosphere at 28 °C, in Roux flasks (Corning, USA) with a surface area of 75 cm<sup>2</sup>, according to the methodology described by Gonzalez et al. [81] The screening of extracellular forms of parasites was carried out using 24-well plates with MTL medium and 5 × 10<sup>4</sup> parasites per well. The products were tested at 1, 10, 25 and 50 μM, prepared from mother aqueous solutions of the compounds, leaving some wells without drugs as control, and were incubated at 28 °C during 72 h before the parasite final count.

#### 4.10. Cell culture and cytotoxicity test

The cytotoxicity tests for macrophages and Vero cells were performed at the Cell Experiment Unit in the “Centro de Instrumentación Científica” of the University of Granada, according to the methodology described below. The experiment was carried out in 96-well plates to be measured in the ELISA reader. The growth inhibition of mammalian cells was studied using macrophages for the three strains of *Leishmania* spp. and Vero cells for *T. cruzi*. J774.2 macrophages (European Collection of Cell Culture – ECACC – number 91051511), which were originally obtained from a tumour in a female BALB/c rat in 1968, were grown in a minimum essential medium (MEM) plus glutamine (2 mM) and supplemented with 20% inactivated fetal bovine serum (FBS). Vero cells (Flow) were grown in Roswell Park Memorial Institute medium (RPMI), which was supplemented with 10% inactivated fetal bovine serum. Both cell cultures were incubated in a humidified 95% air, 5% CO<sub>2</sub> atmosphere at 37 °C for several days.

The products were tested at 50, 100, 200 and 400 μM. First, the cells were sowed in a 96-well plate (2500 cells/well for macrophages and

3500 cells/well for Vero cells) to a volume of 100 μL/well and then were incubated at 37 °C with 5% CO<sub>2</sub> during 24 h. The complexes solutions were prepared in advance corresponding to the average growing cells (RPMI 10% FBS for Vero cells and MEM + Glut 20% FBS for macrophages) at the double of the highest concentration to be tested. The solutions were performed in a sterile bath with the different channels, by adding 100 μL of complex solution or medium (only adding medium in the control wells) to the corresponding well. After that, the plate was incubated at 37 °C with 5% CO<sub>2</sub> for 48 h. Two days after, 20 μL of Alamar Blue dye (10% of the volume of the well) were added to each well and incubated at 37 °C with 5% CO<sub>2</sub> during another day. The whole incubation time once the products were added was 72 h, coinciding with the screening period to have comparable selectivity index (SI) results. Finally, the plate was read with an ELISA reader with Alamar Blue.

#### 4.11. In vivo assays

Forty-eight female CD1 mice (31.2 g body weight and 130 ± 38 mg/dL fasting glycaemia at the beginning of the experimental period) were randomly distributed into 6 groups of 8 animals each. In 5 groups, type I diabetes was induced by the pharmacological administration on consecutive days of two doses of 70 mg/kg body weight of streptozotocin (STZ) as diabetogenic agent [82]. After 7 days, mice shown significant hyperglycaemia (301 ± 65 mg/dL). The experimental groups are described as follows: a) control group: 8 healthy mice; b) diabetic untreated group: 8 STZ diabetic mice; c) diabetic group treated with the ligand: 8 STZ diabetic mice treated with 7-amtp; d) diabetic group treated with compound **1**: 8 STZ diabetic mice treated with compound **1** as glucose lowering agent; e) diabetic group treated with compound **2**: 8 STZ diabetic mice treated with compound **2** as glucose lowering agent; and f) diabetic group treated with compound **3**: 8 STZ diabetic mice treated with compound **3** as glucose lowering agent. The mice were fed control chow diet and were given drinking water ad libitum throughout the experimental period.

The Zn compounds were administered at the dose of 15 mg Zn/kg [83] body weight as dissolved in water (extemporary preparation) using oral gavages (1 ≤ 100 μM) in volumes of 0.1 ml [84,34]. The oral glucose tolerance test was performed obtaining peripheral blood from the tail vein of the mice as described previously [57]. The blood glucose levels were analysed by the use of a glucometer (Accucheck Aviva, Roche).

All the animals were group-housed in metabolism cages. The cages were located in a well ventilated, temperature-controlled room (21 ± 2 °C) with relative humidity ranging from 40 to 60%, and a light–dark period of 12 h. All the experiments were carried out in accordance with Directional Guides Related to Animal Housing and Care (European Council Community, 1986) and all procedures were approved by the Animal Experimentation Ethics Committee of the University of Granada.

#### Declaration of competing interest

There is not any conflict of interest.

#### Acknowledgements

Financial support was given by Junta de Andalucía (Spain) (project number FQM-195, FQM-394 and FQM-1484) and the Spanish Ministry of Science, Innovation and Universities (MCIU/AEI/FEDER, UE) (PGC2018-102052-A-C22 and PGC2018-102052-B-C21) (University Faculty Training Plan – FPU Grants). The authors thank for technical and human support provided by SGiker of UPV/EHU and European funding (ERDF and ESF).

## Abbreviations

7-atp 7-amino[1,2,4]triazolo[1,5-a]pyrimidine  
 7-amtp 7-amino-5-methyl [1,2,4]triazolo[1,5-a]pyrimidine  
 tn 1,3-propanediamine  
 bpym 2,2'-bipyrimidine  
 mal malonate  
 HmtpO 7-hydroxy-5-methyl[1,2,4]triazolo[1,5-a]pyrimidine  
 AMPK $\alpha$  AMP-activated protein kinase  
 ERK2/MAPK1 mitogen-activated protein kinase-1  
 FBS fetal bovine serum  
 GLUT4 glucose transporter type 4  
 GSK-3 $\beta$  glycogen synthase kinase-3  
 HBSS Hank's Balanced Salt Solution  
 HOMO highest occupied molecular orbital  
 IC inhibitory concentration  
 IC<sub>50</sub> half maximal inhibitory concentration  
 IR- $\beta$  insulin receptor  
 LLCT ligand-to-ligand charge transfer  
 LUMO lowest unoccupied molecular orbital  
 MEM Minimal Essential Medium  
 MTL Medium Trypanosome Liquid  
 PFK phosphofructokinase  
 PK pyruvate kinase  
 PL photoluminescence  
 RPMI Roswell Park Memorial Institute  
 SI selectivity index  
 TD-DFT Time Dependent Density Functional Theory

## Appendix A. Supplementary data

Electronic Supplementary Information (ESI) available: Single crystal X-ray diffraction, continuous shape measurements, powder X-ray diffraction, magnetic properties and photoluminescence properties. CCDC numbers 1893521–24, COD numbers 3000220–23. Supplementary data to this article can be found online at doi: <https://doi.org/10.1016/j.jinorgbio.2020.111235>.

## References

- [1] Global Report on Diabetes, World Health Organisation, 2016.
- [2] S. Bastaki, *Int. J. Diab. Metabol.* 13 (2005) 111–134.
- [3] J. Tillner, M. G. Posch, F. Wagner, L. Teichert, Y. Hijazi, C. Einig, S. Keil, T. Haack, M. Wagner, M. Bossart, P. J. Larsen, *Diabetes Obes. Metab.* 21 (2109) 120–128.
- [4] K. Alves de Oliveira, M.D. Moreira Gomes, R. Prado Vasconcelos, E. Sosa de Abreu, R. Soares Fortunato, A.C. Carneiro Loureiro, A.N. Coelho-de-Souza, R.S. Basilio de Oliveira, C.D. Teixeira de Freitas, M. Viana Ramos, A. Cunha de Oliveira, *Biomed. Pharmacother.* 109 (2019) 2342–2347.
- [5] Q. Hu, Q. Niu, H. Song, S. Wei, S. Wang, L. Yao, Y. Li, *Biomed. Pharmacother.* 109 (2019) 876–885.
- [6] K.H. Thompson, J. Lichter, C. Lebel, M.C. Scaife, J.H. McNeill, C. Orvig, *J. Inorg. Biochem.* 13 (2009) 554–558.
- [7] C.E. Heyliger, A.G. Tahiliani, J.H. McNeill, *Science* 227 (1958) 1474–1477.
- [8] J. Jansen, W. Karges, L. Rink, *J. Nutr. Biochem.* 20 (2009) 399–417.
- [9] Y. Song, J. Wang, X.K. Li, L. Cai, *Biomaterials* 18 (2005) 325–332.
- [10] L. Coulston, P. Dandona, *Diabetes* 29 (1980) 665–667.
- [11] A.P. Seale, L.A. de Jesus, S.-Y. Kim, Y.-H. Choi, H.B. Lim, C.-S. Hwang, Y.-S. Kim, *Biotechnol. Lett.* 27 (2005) 221–225.
- [12] K.H. Thompson, J. Lichter, C. Lebel, M.C. Scaife, J.H. McNeill, C. Orvig, *J. Inorg. Biochem.* 13 (2009) 554–558.
- [13] C.E. Heyliger, A.G. Tahiliani, J.H. McNeill, *Science* 227 (1985) 1474–1477.
- [14] J. Jansen, W. Karges, L. Rink, *J. Nutr. Biochem.* 20 (2009) 399–417.
- [15] P.O. Anikeeva, J.E. Halpert, M.G. Bawendi, V. Bulovic, *Nano Lett.* 9 (2009) 2532–2536.
- [16] P.T. Snee, R.C. Somers, G. Nair, J.P. Zimmer, M.G. Bawendi, D.G. Nocera, *J. Am. Chem. Soc.* 128 (2006) 13320–13321.
- [17] J.-S. Hu, Y.-J. Shang, X.-Q. Yao, L. Qin, Y.-Z. Li, Z.-J. Guo, H.-G. Zheng, Z.-L. Xue, *Cryst. Growth Des.* 10 (2010) 2676–2684.
- [18] M. Melchior, K.H. Thompson, J.M. Jong, S.J. Rettig, E. Shuter, V.G. Yuen, Y. Zhou, J.H. McNeill, C. Orvig, *Inorg. Chem.* 38 (1999) 2288–2293.
- [19] C.C. McLauchlan, J.D. Hooker, M.A. Jones, Z. Dymon, E.A. Backhus, B.A. Greiner, N.A. Dorner, M.A. Youkhana, L.M. Manus, *J. Inorg. Biochem.* 104 (2010) 274–281.
- [20] E. Lodyga-Chruscinska, G. Micera, E. Garribba, *Inorg. Chem.* 50 (2011) 883–899.
- [21] P.T. Snee, R.C. Somers, G. Nair, J.P. Zimmer, M.G. Bawendi, D.G. Nocera, *J. Am. Chem. Soc.* 128 (2006) 13320.
- [22] J.-S. Hu, Y.-J. Shang, X.-Q. Yao, L. Qin, Y.-Z. Li, Z.-J. Guo, H.-G. Zheng, Z.-L. Xue, *Cryst. Growth Des.* 10 (2010) 2676.
- [23] A.B. Caballero, A. Rodríguez-Dieguez, E. Barea, M. Quiros, J.M. Salas, *CrystEngComm* 12 (2010) 3038–3045.
- [24] A.J. Calahorra, A. Peñas-Sanjuan, M. Melguizo, D. Fairen-Jimenez, G. Zaragoza, B. Fernández, A. Salinas-Castillo, A. Rodríguez-Dieguez, *Inorg. Chem.* 52 (2013) 546–548.
- [25] Z. Xia, Q. Wei, Q. Yang, C. Qiao, S. Chen, *CrystEngComm* 15 (2013) 86.
- [26] B. Fernández, A. Gómez-Víchez, C. Sánchez-González, J. Bayón, E. San Sebastian, S. Gómez-Ruiz, C. López-Chaves, P. Aranda, J. Llopis, A. Rodríguez-Dieguez, *New J. Chem.* 40 (2016) 5387–5393.
- [27] V. Guillermin, D. Kim, J.F. Eubank, R. Luebke, X. Liu, K. Adil, M.S. Lah, M. Eddaoudi, *Chem. Soc. Rev.* 43 (2014) 6141–6172.
- [28] M. Eddaoudi, D.F. Sava, J.F. Eubank, K. Adil, V. Guillermin, *Chem. Soc. Rev.* 44 (2015) 228–249.
- [29] J.M. Mendez-Arriaga, I. Oyarzabal, G. Escolano, A. Rodríguez-Dieguez, M. Sanchez-Moreno, J.M. Salas, *J. Inorg. Biochem.* 180 (2018) 26–32.
- [30] A. Dominguez-Martin, M. Brandi-Blanco, A. Matilla-Hernandez, H. El Bakkali, V.M. Nurchi, J.M. Gonzalez-Perez, A. Castineiras, J. Niclos-Gutierrez, *Coord. Chem. Rev.* 257 (2013) 2814–2838.
- [31] A.B. Caballero, A. Rodríguez-Dieguez, L. Lezama, J.M. Salas, *Cryst. Growth Des.* 12 (2012) 3583–3593.
- [32] A.B. Caballero, A. Rodríguez-Dieguez, I. Vidal, J.A. Dobado, O. Castillo, L. Lezama, J.M. Salas, *Dalton Trans.* 41 (2012) 1755–1764.
- [33] A.B. Caballero, C. Marin, I. Ramirez-Macias, A. Rodríguez-Dieguez, M. Quiros, J.M. Salas, M. Sanchez-Moreno, *Polyhedron* 33 (2012) 137–144.
- [34] J.M. Méndez-Arriaga, A. Rodríguez-Dieguez, M. Sánchez-Moreno, *Polyhedron* 176 (2020) 114272.
- [35] A.B. Caballero, J.K. MacLaren, A. Rodríguez-Dieguez, I. Vidal, J.A. Dobado, J.M. Salas, C. Janiak, *Dalton Trans.* 40 (2011) 11845–11855.
- [36] A.B. Caballero, A. Rodríguez-Dieguez, M. Quiros, L. Lezama, J.M. Salas, *Inorg. Chim. Acta* 378 (2011) 194–201.
- [37] I. Łakomska, M. Fandzloch, *Coord. Chem. Rev.* 327–328 (2016) 221–241.
- [38] M.P. DeNinno, S.W. Wright, J.B. Etienne, T.V. Olson, B.N. Rocke, J.W. Corbett, D.W. Kung, K.J. DiRico, K.M. Andrews, M.L. Millham, J.C. Parker, W. Esler, M. van Volkenburg, D.D. Boyer, K.L. Houseknecht, S.D. Doran, *Bioorg. Med. Chem. Lett.* 22 (2012) 5721–5726.
- [39] J. E. Campbell, P. Jones and M. C. Hewitt, US 20120178748.
- [40] U. S. Soerensen, B. L. Eriksen, C. Hougaard, D. Stroebaek and P. Christophersen, WO 2010112486.
- [41] G. Liu, Z. Xin, P. R. Kym and A. J. Souers, WO 2008134690.
- [42] A. B. Mikkilineni, N. Murugesan and G. Yu, US 20060287342.
- [43] R.C. Evans, P. Douglas, C.J. Winscom, *Coord. Chem. Rev.* 250 (2006) 2093.
- [44] Q.-D. Liu, R. Wang, S. Wang, *Dalton Trans.* (2004) 2073–2079.
- [45] A. Barbieri, G. Accorsi, N. Armaroli, *Chem. Commun.* (2008) 2185.
- [46] X. Yang, D. Yan, *Adv. Opt. Mater.* 4 (2016) 897–905.
- [47] A.A. García-Valdivia, J.M. Seco, J. Cepeda, A. Rodríguez-Dieguez, *Inorg. Chem.* 56 (2017) 13897–13912.
- [48] X. Yang, D. Yan, *Chem. Sci.* 7 (2016) 4519–4526.
- [49] J.M. Seco, S. Pérez-Yáñez, D. Briones, J.A. García, J. Cepeda, A. Rodríguez-Dieguez, *Cryst. Growth Des.* 17 (2017) 3893–3906.
- [50] Y. Yang, K.Z. Wang, D. Yan, *ACS Appl. Mater. Interfaces* 8 (2016) 15489–15496.
- [51] Y.X. Sun, W.Y. Sun, *CrystEngComm* 17 (2015) 4045–4063.
- [52] R.C. Evans, P. Douglas, C.J. Winscom, *Coord. Chem. Rev.* 250 (2006) 2093–2126.
- [53] A. Barbieri, G. Accorsi, N. Armaroli, *Chem. Commun.* (2008) 2185–2193.
- [54] J.M. Salas, A.B. Caballero, G.M. Esteban-Parra, J.M. Méndez-Arriaga, *Curr. Med. Chem.* 24 (2017) 2796–2806.
- [55] A.B. Caballero, A. Rodríguez-Dieguez, M. Quirós, J.M. Salas, Ó. Huertas, I. Ramírez-Macias, F. Olmo, C. Martin, G. Chaves-Lemaire, R. Gutierrez-Sánchez, M. Sánchez-Moreno, *Eur. J. Med. Chem.* 85 (2014) 526–534.
- [56] A.B. Caballero, C. Marin, I. Ramirez-Macias, A. Rodríguez-Dieguez, M. Quirós, J.M. Salas, M. Sánchez-Moreno, *Polyhedron* 33 (2012) 137–144.
- [57] M.E. López-Viseras, B. Fernández, S. Hilfiker, C.S. González, J.L. González, A.J. Calahorra, E. Colacio, A. Rodríguez-Dieguez, *J. Inorg. Biochem.* 131 (2014) 64–67.
- [58] M. Doumas, K. Imprialos, K. Stavropoulos, A. Reklou, A. Sachinidis, V.G. Athyros, *Curr. Pharm. Des.* 24 (2018) 1879–1886.
- [59] Y. Zhang, K. Thai, T. Jin, M. Woo, R.E. Gilbert, *Sci. Rep.* 8 (2018) 1.
- [60] C. Ning, H. Jun, Z. Gui-Yun, A. Xiao-Ying, S. Jing-Jing, O. Qin, Y. Yong-Hui, *Chin. Pharmacol. Bull.* 34 (2018) 112–117.
- [61] S.A. Barbati, C. Colussi, L. Bacci, A. Aiello, A. Re, E. Stigliano, A.M. Isidori, C. Grassi, A. Pontecorvi, A. Farsetti, C. Gaetano, S. Nanni, *Endocrinology* 158 (2017) 405–411.
- [62] Y. Gan, N. Dang, Z. Qu, R. Shi, L. Ding, L. Wang, S. Pang, *Exp. Clin. Endocrinol. Diab.* 123 (2015) 371–375.
- [63] P. Ranasinghe, S. Piger, P. Galappaththy, P. Katulanda, G.R. Constantine, *DARU J. Pharm. Sci.* 23 (2015) 44.
- [64] H. Kano, Y. Makisumi, *Chem. Pharm. Bull.* 6 (1958) 583–586.
- [65] Bruker Apex2, Bruker AXS Inc., Madison, Wisconsin, USA, 2004.
- [66] G.M. Sheldrick, SADABS, Program for Empirical Adsorption Correction, Institute for Inorganic Chemistry, University of Göttingen, Germany, 1996.
- [67] A. Altomare, M.C. Burla, M. Camilla, G.L. Casciarano, C. Giacovazzo, A. Guagliardi, A.G.G. Moliterni, G. Polidori, R. Spagna, *J. Appl. Crystallogr.* 32 (1999) 115–119.
- [68] G. M. Sheldrick, *Acta Cryst C* (2015) 713–8.

- [69] M.J. Frisch, G.W. Trucks, H.B. Schlegel, G.E. Scuseria, M.A. Robb, J.R. Cheeseman, G. Scalmani, V. Barone, B. Mennucci, G.A. Petersson, H. Nakatsuji, M. Caricato, X. Li, H.P. Hratchian, A.F. Izmaylov, J. Bloino, G. Zheng, J.L. Sonnenberg, M. Hada, M. Ehara, K. Toyota, R. Fukuda, J. Hasegawa, M. Ishida, T. Nakajima, Y. Honda, O. Kitao, H. Nakai, T. Vreven, J.A. Montgomery Jr., J.E. Peralta, F. Ogliaro, M. Bearpark, J.J. Heyd, E. Brothers, K.N. Kudin, V.N. Staroverov, R. Kobayashi, J. Normand, K. Raghavachari, A. Rendell, J.C. Burant, S.S. Iyengar, J. Tomasi, M. Cossi, N. Rega, J.M. Millam, M. Klene, J.E. Knox, J.B. Cross, V. Bakken, C. Adamo, J. Jaramillo, R. Gomperts, R.E. Stratmann, O. Yazyev, A.J. Austin, R. Cammi, C. Pomelli, J.W. Ochterski, R.L. Martin, K. Morokuma, V.G. Zakrzewski, G.A. Voth, P. Salvador, J.J. Dannenberg, S. Dapprich, A.D. Daniels, O. Farkas, J.B. Foresman, J.V. Ortiz, J. Cioslowski, D.J. Fox, Gaussian 09, Revision A.02, Gaussian, Inc., Wallingford, CT, 2009.
- [70] A.D. Becke, *J. Chem. Phys.* 98 (1993) 5648–5652.
- [71] B. Miehlisch, A. Savin, H. Stoll, H. Preuss, *Chem. Phys. Lett.* 157 (1989) 200–206.
- [72] C. Lee, W. Yang, R.G. Parr, *Phys. Rev. B* 37 (1988) 785–789.
- [73] L. Noodleman, D.A. Case, A. Aizman, *J. Am. Chem. Soc.* 110 (1988) 1001–1005.
- [74] P.J. Hay, W.R. Wadt, *J. Chem. Phys.* 82 (1985) 270–283.
- [75] W.R. Wadt, P.J. Hay, *J. Chem. Phys.* 82 (1985) 284–298.
- [76] P.J. Hay, W.R. Wadt, *J. Chem. Phys.* 82 (1985) 299–310.
- [77] X. Shuhong, W. Chunlei, W. Zhuyuan, C. Yiping, *J. Mol. Model.* 20 (2014) 2184.
- [78] Z. Kangcheng, L. Xuewen, D. Hong, C. Hui, Y. Fengcun, J. Liangnian, *J. Mol. Struct. Theochem.* 626 (2003) 295–304.
- [79] N.M. O'Boyle, A.L. Tenderholt, K.M. Langner, *J. Comput. Chem.* 29 (2008) 839–845.
- [80] R. Dennington, T. Keith, J. Millam, GaussView, Version 5, Semichem Inc., Shawnee Mission, KS, 2009.
- [81] P. González, C. Marín, I. Rodríguez-González, A.B. Hitos, M.J. Rosales, M. Reina, J.G. Díaz, A. González-Coloma, M. Sánchez-Moreno, *Int. J. Antimicrob. Agents* 25 (2005) 136–141.
- [82] J. Ventura-Sobrevilla, V.D. Boone-Villa, C.N. Aguilar, R. Román-Ramos, E. Vega-Ávila, E. Campos-Sepúlveda, F. Alarcón-Aguilar, *Proc. West. Pharmacol. Soc.* 54 (2011) 5–9.
- [83] D. Briones, B. Fernández, A.J. Calahorra, D. Fairen-Jimenez, R. Sanz, F. Martínez, G. Orcajo, E.S. Sebastián, J.M. Seco, C.S. González, J. Llopis, A. Rodríguez-Diéguez, *Cryst. Growth Des.* 16 (2016) 537–540.
- [84] S. Tunali, R. Yanardag, *Pharmacol. Res.* 53 (2006) 271–277.